Spin saturation artifact correction using slice-to-volume registration motion estimates for fMRI time series

Roshni Bhagalia[a)]
Department of Electrical Engineering and Computer Science, University of Michigan, 1301 Beal Avenue, Ann Arbor, Michigan 48109 and Department of Radiology, University of Michigan Medical School, Ann Arbor, Michigan 48109

Boklye Kim
Department of Radiology, University of Michigan Medical School, Ann Arbor, Michigan 48109

Evaluation of functional magnetic resonance imaging (fMRI) as a reliable clinical imaging tool requires accurate assessment and correction of head motion artifacts. As the correction of bulk head motion is vital, the loss of signal strength from the confounding effect of head motion on spin magnetization may be an additional factor in activation analysis error. This study focuses on the evaluation and correction of the spin saturation artifact that occurs when parts of adjacent slices are selected due to changing head positions in single-shot multislice acquisitions. As a consequence of head movement, the acquired slices constituting a fMRI volume are no longer parallel to each other and the spin magnetization in fMRI voxels becomes dependent on head motion history. Motion corrections applying the same rigid motion estimates to all the slices in a volume may not be a reasonable approximation in cases where the magnitude of head motion exceeds a subvoxel range. For realistic ranges of motion in fMRI, an accurate estimate of rigid motion parameters for each echo planar imaging (EPI) slice is essential to correctly register voxel intensities. Previously we have implemented the map-slice-to-volume (MSV) motion correction method that maps each slice in a time series onto a reference anatomical volume, which proved to be effective in improving activation detection. To correctly evaluate the motion dependence of spin magnetization, each voxel is tracked with movement history that is available from MSV motion estimates. Relatively low in resolution, EPI voxels are composed of varying mixtures of white matter (WM), gray matter (GM), and cerebrospinal fluid (CSF) and variations in the tissue composition give rise to voxel intensities that are functions of tissue $T1$ properties. We have developed a weighted-average spin saturation (WASS) correction method that can handle full rigid motion and account for the mélange of different brain tissue isochromats at each EPI voxel location. We evaluated the effect of spin saturation artifacts and the performance of the WASS correction using simulated fMRI time series synthesized with known true activation, motion, and the associated spin saturation artifact. Two different ranges of head rotations, $[-5,5]$ and $[-2,2]$ deg, were introduced and the effect of the spin saturation artifact was quantified to show 18% and 13% reduction in activation detection rate, respectively. Following the MSV motion and WASS correction, results indicate that WASS correction can improve activation detection by 17% relative to MSV only correction. © *2008 American Association of Physicists in Medicine.* [DOI: 10.1118/1.2826555]

Key words: spin saturation artifacts, fMRI time series, slice-to-volume registration

I. I INTRODUCTION

Functional magnetic resonance imaging (fMRI) is a noninvasive tool for imaging brain function. The functionality of the brain relative to a particular stimulus is assessed by measuring stimulus triggered blood oxygenation level dependent (BOLD) signal intensity changes along a series of MR images acquired for the duration of the activation study, i.e., a fMRI time series. However, due to subject head motion, voxel intensities may be altered, causing signal intensity changes dependent on positions of the head with respect to the scanner.[1] The use of head restraints is not only impractical for patient studies in which discomfort may cause adverse reactions but also not a satisfactory solution to motion

problems. Since the activation hypotheses for the various brain regions are tested using statistical testing[2–4] to identify significant fMRI signal changes, undesired signal variation from head motion apart from BOLD intensity changes would skew the activation analyses.

This work focuses on the confounding effect of head motion on spin magnetization, leading to an additional increase in signal modulation that is not related to the BOLD effect. Most fMRI time series are acquired by a multislice scheme using single shot echo planar imaging (EPI). Single shot acquisition of an EPI slice makes it possible to safely neglect head motion during a slice excitation. However, due to changes in head position during the multislice acquisition, slices in the volume are no longer parallel to each other.

Thus, some nuclear spins are reexcited before being allowed sufficient time to recover to their equilibrium states causing spin saturation. This motion dependant alteration in spin magnetization makes the signal intensity variation in overlapping slice areas a function of the subject's movement history. The spin saturation artifact, also called spin history artifact in the literature,[1,5] may be an additional factor in false detection of fMRI signals in activation analysis by statistical inference.

Although recognized as a potential problem in fMRI activation analyses,[1] the effect of spin saturation artifacts on activation detection has not been investigated with the capability to follow voxel positions accurately. The spin saturation artifact at a particular single tissue voxel is a function of head position relative to B_0, repetition time (TR) and echo time (TE), the effective flip angle, and $T1$-dependent signal amplitude. Since EPI data are acquired at low spatial resolution, each EPI voxel can be approximated by a mixture of gray matter (GM), white matter (WM), and cerebrospinal fluid (CSF) isochromats. Patient head motion may result in a loss of equilibrium magnetization states for some or all isochromats contributing to a particular EPI voxel, due to excitation at irregular time intervals.

The approach to correct spin-history artifacts by Friston *et al.*[1] uses regression of intensities using motion parameters obtained from volume to volume registration. Volume-to-volume registration schemes assume that all slices in an acquired volume are aligned parallel to each other and may not provide a reasonable approximation of inter-slice head motion. This precludes the use of such volumetric motion estimates to assess and correct spin saturation artifacts induced by relative changes in slice positions in the same EPI volume. Muresan *et al.*[5] have proposed a spin correction scheme that is to be applied prior to motion estimation. However their method is also restricted to the correction of spin saturation effects arising due to head motion between volume acquisitions only.

In this study, we propose to use rigid motion estimates with six degrees of freedom obtained from our map-slice-to-volume[6] (MSV) motion correction technique, which maps each EPI slice onto a higher resolution anatomical volume acquired from the same subject. This mapping can be used to track the motion dependent, irregular time intervals between consecutive slice excitations at the higher resolution of the anatomical volume. Since anatomical data voxels are sampled finely enough to be approximated as tissue isochromats, they can be used to estimate unknown fractions of GM, WM, and CSF contributing to each mapped EPI voxel. Motion estimates from MSV, slice geometry, TR, TE, and effective flip angles at each voxel location are then used to identify voxels with spin saturation artifacts. To approximate spin saturation correction factors for EPI voxels, a weighted-average spin saturation (WASS) correction is introduced. To alleviate partial volume effects, the spin saturation correction factor for each affected EPI voxel is approximated by a convex combination of the correction factors of its constituent brain tissue isochromats as identified by its mapping onto the anatomical volume.

This work presents (i) the spin saturation effect using mathematical expressions and (ii) the WASS correction which compensates EPI voxels affected by spin saturation, by approximating the ratios of changes in their intensities attributable to spin saturation, using known time series parameters and motion estimates. To evaluate our method, two realistic fMRI time series with known rigid motion and corresponding spin saturation artifacts were simulated. The ranges of motion introduced in the two time series were [−5,5] and [−2,2] deg, respectively. Activation was introduced in manually selected brain regions assuming an epoch based experimental paradigm with a box-car stimulus sequence. Motion estimates from MSV were used to correct the simulated data for spin saturation related voxel intensity variation. Receiver operating characteristic (ROC) curves were generated using activation maps for both simulated times series after MSV motion correction with and without WASS correction, as well as for the simulated ground truth. Results suggest that weighted average spin saturation artifact correction with retrospective MSV motion estimation may have a significant role in improving activation detection.

II. THEORY

II.A. Mathematical expressions for spin saturation artifacts in single tissue voxels

To acquire a multislice fMRI time series, longitudinal magnetizations of spins in slice-like regions of the subject's brain are selectively excited and flipped onto the transverse plane using an α-angle radio frequency (rf) pulse. It has been established that the intensity of a tissue isochromat at a given coordinate in an acquired MR volume is proportional to the effective flip angle and to the magnetization component in the XY plane, at that location.[7] For now we focus on the effect of patient head motion on the intensity of a single tissue isochromat. Let $m_z^0(\vec{v})$ be the initial magnetization (at rest) of a particular tissue isochromat at location $\vec{v} \in R^3$, characterized by a single tissue with time constants $T1$ and $T2$. Let $m_{z,i}^-(\vec{v})$ be the longitudinal magnetization just before the ith flip angle pulse with effective flip angle $\alpha_i(\vec{v})$ The longitudinal magnetization $m_{z,i}^+(\vec{v})$ just after the ith excitation pulse is given by

$$m_{z,i}^+(\vec{v}) = m_{z,i}^-(\vec{v})\cos(\alpha_i(\vec{v})), \qquad (1)$$

where $m_{z,i}^-(\vec{v}) = m_z^0(\vec{v})$. Let $t_i, i = 1,2,\ldots$ be the time interval between the ith and $i+1$th consecutive excitation of the tissue isochromat, then the longitudinal magnetization between excitations recovers according to

$$m_{z,i+1}^-(\vec{v}) = m_{z,i}^+(\vec{v})e^{-t_i/T1} + m_z^0(\vec{v})(1 - e^{-t_i/T1})$$
$$= m_{z,i}^-(\vec{v})\cos(\alpha_i(\vec{v}))e^{-t_i/T1} + m_z^0(\vec{v})(1 - e^{-t_i/T1}). \quad (2)$$

The brain volume of interest is repeatedly excited M times before conducting the activation study so as to force all magnetization vectors to achieve an incoherent steady state.[8] In such a state, if each tissue isochromat is excited every TR,

$m_{z,i+1}^-(\vec{v}) = m_{z,i}^-(\vec{v}) = m_z^{ss}(\vec{v}), \forall i \geq M$ This steady state magnetization $m_z^{ss}(\vec{v})$ can be expressed in terms of the initial magnetization using Eq. (2),

$$m_{z,M+1}^-(\vec{v}) = m_{z,M}^-(\vec{v})\cos(\alpha_M(\vec{v}))e^{-TR/T1} + m_z^0(\vec{v})(1 - e^{-TR/T1})$$

$$= m_z^{ss}(\vec{v}), \ \alpha_i(\vec{v}) = \alpha(\vec{v})\forall_i$$

$$\Rightarrow m_z^{ss}(\vec{v}) = m_z^0(\vec{v})f_{ss}(\vec{v}),$$

$$\text{where } f_{ss}(\vec{v}) \triangleq \frac{1 - e^{-TR/T1}}{1 - \cos(\alpha(\vec{v}))e^{-TR/T1}}; i \geq M. \quad (3)$$

Hence, in the absence of head motion the artifact free intensity I_{true} is proportional to the transverse magnetization, $m_{xy}^{ss}(\vec{v}) = m_z^{ss}(\vec{v})\sin(\alpha(\vec{v}))$,

$$I_{true}(\vec{v}) \propto m_{xy}^{ss}(\vec{v})e^{-TE/T2}$$

$$= m_z^0(\vec{v})\frac{1 - e^{-TR/T1}}{1 - \cos(\alpha(\vec{v}))e^{-TR/T1}}\sin(\alpha(\vec{v}))e^{-TE/T2}. \quad (4)$$

In the presence of head motion between slice acquisitions, EPI slices in a volume are not parallel to each other. Hence, the time difference between the successive excitations of some spins cannot be maintained at TR, causing the incoherent steady state established by Eq. (3) to break down. Thus, Eq. (4) is rarely an accurate representation of isochromatic tissue intensities in an fMRI study. In particular, the intensity of a given tissue isochromat will drop if less than TR ms have elapsed since its last excitation causing the longitudinal magnetization at that location to be reexcited before relaxing to $m_z^{ss}(\vec{v})$. The effect of n irregularly spaced excitations on $m_{z,n}^-(\vec{v})$ can be found by repeatedly using Eqs. (1) and (2). Specifically, it can be shown that

$$m_{z,n}^-(\vec{v}) = m_z^0(\vec{v})f_n(\vec{v}), \quad (5)$$

where $f_n(\vec{v})$, a function of tissue $T1$, the effective flip angles $\alpha_i(\vec{v}), i=1,2,\ldots,n-1$, and previous head positions via $t_i, i=1,2,\ldots,n-1$, is recursively given by

$$f_{i+1}(\vec{v}) = f_i(\vec{v})\cos(\alpha_i(\vec{v}))e^{-t_i/T1} + (1 - e^{-t_i/T1}),$$
$$i = 1,2,\ldots, \quad (6)$$

with $f_1(\vec{v}) = (1 - e^{-TR/T1})/(1 - \cos(\alpha(\vec{v}))e^{-TR/T1})$, assuming that the isochromat was initially in its incoherent steady state given by Eq. (3). The corresponding observed intensity affected by the spin saturation phenomenon, $I_{obvs}(\vec{v},n)$, is proportional to the transverse magnetization $m_{xy,n}(\vec{v})$,

$$I_{obvs}(\vec{v},n) \propto m_{xy,n}(\vec{v})e^{-TE/T2} = m_z^0(\vec{v})f_n(\vec{v})\sin(\alpha_n(\vec{v}))e^{-TE/T2}. \quad (7)$$

The recursive Eq. (6) is valid only for tissue isochromats of small voxels. However, to gain temporal resolution, fMRI scans typically have relatively large voxel sizes. Thus, the intensity of each fMRI voxel is proportional to the average transverse magnetization of a mixture of GM, WM, and CSF isochromats.

II.B. Spin saturation artifact correction for EPI voxels

Spin saturation artifacts are a direct consequence of head motion and voxels affected by them can be identified using head trajectory estimates, head geometry, and fMRI time series attributes. As noted earlier, EPI voxels have low spatial resolution. Thus, the intensity of a single EPI voxel in a fMRI time series reflects the average transverse magnetization over a small brain volume made up of a mélange of different brain tissue. Consequently, the effective time constants $T1^{epi}$ and $T2^{*epi}$ of the EPI voxel cannot be estimated satisfactorily using a single brain tissue.

Consider the acquisition of a fMR time series using EPI with repetition time TR, echo time TE, and α-angle rf pulses. Let the time series contain V volumes with S slices in each volume. Let $s, s=1,2,\ldots,S$ index the slices in acquisition order in a given EPI volume $v, v=1,2,\ldots,V$. The integer $n_{epi}=(v-1)S+s$ indexes the total number of slices in the EPI time series by acquisition order. In the presence of subject head motion, the observed intensity of an EPI voxel at coordinate $\vec{u} \in R^3$ in slice n_{epi} of the time series is given by

$$I_{obvs}(\vec{u},n_{epi}) \propto m_{z,epi}^-(\vec{u},n_{epi})\sin(\alpha(\vec{u}))e^{-TE/T2^{*epi}},$$
$$\text{where } n_{epi} = 1,2,\ldots,V \times S. \quad (8)$$

$m_{z,epi}^-(\vec{u},n_{epi})$ is the longitudinal magnetization of the EPI voxel at location $\vec{u}$ just before the excitation pulse for the n_{epi}^{th} slice of the time series. Due to subject head motion, the S slices in each EPI volume will no longer be parallel to each other. Consequently, spins in some portion of these slices will be excited at irregular time intervals causing them to deviate from their induced steady state. This transitory response of some spin magnetizations will result in spin saturation, causing the longitudinal magnetization at a given coordinate location to vary across volumes.

However, in the absence of subject motion, the magnetization vectors in the entire brain volume can be assumed to be in an induced incoherent steady state. The intensity of an EPI voxel at location $\vec{u}$ assuming no motion is given by

$$I_{true}(\vec{u}) \propto m_{z,epi}^{ss}(\vec{u})\sin(\alpha(\vec{u}))e^{-TE/T2^{*epi}}, \quad (9)$$

where $m_{z,epi}^{ss}(\vec{u})$ is the incoherent steady state magnetization of the EPI voxel. In the absence of subject motion and signal noise this steady state magnetization at a given location $\vec{u}$ will not change across the time series volumes due to spin saturation.

The observed intensity of an EPI time series voxel affected by spin saturation is related to that of a motion-free EPI time series of the same subject, obtained using the same timing and acquisition parameters, by

$$I_{true}(\vec{u}) = I_{obvs}(\vec{u},n_{epi})\frac{m_{z,epi}^{ss}(\vec{u})}{m_{z,epi}^-(\vec{u},n_{epi})}. \quad (10)$$

Thus, spin saturation artifacts can be detected and corrected, if we can approximate the ratio $m_{z,epi}^{ss}(.)/m_{z,epi}^-(.)$ at each EPI voxel location. Since such a spin saturation correction mechanism will appropriately scale observed intensity values

$I_{\text{obvs}}(.)$, it will be unable to correct spin saturation at locations where the artifact is severe enough to make the observed intensity zero.

For brevity, we assume without deliberation, the existence of a registration scheme that can obtain reasonably accurate head motion estimates by registering each EPI slice onto a high resolution anatomical MR volume of the same patient.[6] Further, these motion estimates can be used to map every large EPI voxel onto a K neighborhood of finer anatomical volume voxels. Specific details of such a registration process are outlined in Sec. III B.

If we approximate the numerous infinitesimally small GM, WM, and CSF isochromats underlying each mapped EPI voxel by the K neighborhood of "small" finite sized voxels from the anatomical volume with corresponding time constants $T1_{\text{GM}}$, $T1_{\text{WM}}$, and $T1_{\text{CSF}}$; we can express the longitudinal magnetization of the EPI voxel at coordinate $\vec{u} \in R^3$ as the average magnetization computed over this neighborhood

$$m_{z,\text{epi}}^0(\vec{u}) \approx \frac{1}{K} \sum_{\vec{v}_k \in N(\vec{u})} m_z^0(\vec{v}_k),$$

$$m_{z,\text{epi}}^{\text{ss}}(\vec{u}) \approx \frac{1}{K} \sum_{\vec{v}_k \in N(\vec{u})} m_z^{\text{ss}}(\vec{v}_k),$$

and

$$m_{z,\text{epi}}^-(\vec{u},n_{\text{epi}}) \approx \frac{1}{K} \sum_{\vec{v}_k \in N(\vec{u})} m_{z,n_k}^-(\vec{v}_k); \quad n_k \le n_{\text{epi}}, \quad (11)$$

where $N(\vec{u})$ denotes the neighborhood of K finer voxels. $m_{z,\text{epi}}^0(\vec{u})$ is the initial (at rest) magnetization of the EPI voxel at $\vec{u}$, $m_{z,\text{epi}}^{\text{ss}}(\vec{u})$ is its incoherent steady state magnetization assuming no head motion, and $m_{z,\text{epi}}^-(\vec{u},n_{\text{epi}})$ is the longitudinal magnetization just before the excitation of the $n_{\text{epi}}^{\text{th}}$ EPI slice at time point $t_{n_{\text{epi}}}$. The number of consecutive excitations n_k for an approximated isochromat is the number of times series slices that were mapped on to that isochromat up to time $t_{n_{\text{epi}}}$. The time between consecutive excitations $t_1, t_2, \ldots, t_{n_k}$ is given by the time elapsed between the excitation of these n_k EPI slices.

Further, along the lines of Eqs. (3) and (5) we define unknown correction factors $f_{\text{ss}}^{\text{wa}}(\vec{u})$ and $f_{n_{\text{epi}}}^{\text{wa}}(\vec{u},n_{\text{epi}})$ such that, for an EPI voxel at $\vec{u}$,

$$m_{z,\text{epi}}^{\text{ss}}(\vec{u}) \triangleq m_{z,\text{epi}}^0(\vec{u}) f_{\text{ss}}^{\text{wa}}(\vec{u}) \text{ and}$$

$$m_{z,\text{epi}}^-(\vec{u},n_{\text{epi}}) \triangleq m_{z,\text{epi}}^0(\vec{u}) f_{n_{\text{epi}}}^{\text{wa}}(\vec{u}). \quad (12)$$

Approximating the longitudinal magnetizations $m_{z,\text{epi}}(.)$ above by the approximations in Eq. (11) gives

$$f_{\text{ss}}^{\text{wa}}(\vec{u}) \approx \hat{f}_{\text{ss}}^{\text{wa}}(\vec{u}) = \sum_{\vec{v}_k \in N(\vec{u})} \frac{m_z^{\text{ss}}(\vec{v}_k)}{\sum_{\vec{v}_j \in N(\vec{u})} m_z^0(\vec{v}_j)}$$

and

$$f_{n_{\text{epi}}}^{\text{wa}}(\vec{u}) \approx \hat{f}_{n_{\text{epi}}}^{\text{wa}}(\vec{u}) = \sum_{\vec{v}_k \in N(\vec{u})} \frac{m_{z,n_k}^-(\vec{v}_k)}{\sum_{\vec{v}_j \in N(\vec{u})} m_z^0(\vec{v}_j)}. \quad (13)$$

Since the anatomical volume voxels are approximated as GM, WM, and CSF isochromats, we can use Eqs. (3) and (5) to estimate the two correction factors

$$\hat{f}_{\text{ss}}^{\text{wa}}(\vec{u}) = \sum_{\vec{v}_k \in N(\vec{u})} \frac{m_z^0(\vec{v}_k)}{\sum_{\vec{v}_j \in N(\vec{u})} m_z^0(\vec{v}_j)} f_{\text{ss}}(\vec{v}_k)$$

and

$$\hat{f}_{n_{\text{epi}}}^{\text{wa}}(\vec{u}) = \sum_{\vec{v}_k \in N(\vec{u})} \frac{m_z^0(\vec{v}_k)}{\sum_{\vec{v}_j \in N(\vec{u})} m_z^0(\vec{v}_j)} f_{n_k}(\vec{v}_k), \quad (14)$$

where the incoherent steady state factors f_{ss} are given by Eq. (3). The spin saturation dependence of $\hat{f}_{n_{\text{epi}}}^{\text{wa}}$ is captured by the f_{n_k} factors, given by the recursion in Eq. (6) using time constants $T1_{\text{GM}}$, $T1_{\text{WM}}$, or $T1_{\text{CSF}}$ as appropriate.

As each anatomical volume voxel has the same size and the initial magnetization of an isochromat is proportional to its proton density ρ_0, the equilibrium magnetization m_z^0 can be replaced by ρ_0 in Eq. (14). Further, as only relative proton density values of GM, WM, and CSF up to a common factor are required, relative proton densities ρ_0 (dependent on tissue water content) $\rho_{0,\text{GM}}=0.80$, $\rho_{0,\text{WM}}=0.72$, and $\rho_{0,\text{CSF}}=1.0$ can be used

$$\hat{f}_{\text{ss}}^{\text{wa}}(\vec{u}) = \sum_{\vec{v}_k \in N(\vec{u})} \frac{\rho_0(\vec{v}_k)}{\sum_{\vec{v}_j \in N(\vec{u})} \rho_0(\vec{v}_j)} f_{\text{ss}}(\vec{v}_k)$$

and

$$\hat{f}_{n_{\text{epi}}}^{\text{wa}}(\vec{u}) = \sum_{\vec{v}_k \in N(\vec{u})} \frac{\rho_0(\vec{v}_k)}{\sum_{\vec{v}_j \in N(\vec{u})} \rho_0(\vec{v}_j)} f_{n_k}(\vec{v}_k). \quad (15)$$

Finally, using Eqs. (10), (12), and (13) I_{true} can be approximated by

$$\hat{I}_{\text{true}}(\vec{u},n_{\text{epi}}) = I_{\text{obvs}}(\vec{u},n_{\text{epi}}) \frac{\hat{f}_{\text{ss}}^{\text{wa}}(\vec{u})}{\hat{f}_{n_{\text{epi}}}^{\text{wa}}(\vec{u})}. \quad (16)$$

In summary, the estimate of $\hat{I}_{\text{true}}(\vec{u},n_{\text{epi}})$ uses knowledge of approximate tissue $T1$ and ρ_0 values at the resolution of the anatomical volume, time series repetition time TR, the number of EPI volumes V, the number of slices per volume S, and an estimate of the effective flip angle at each anatomical volume voxel grid location. The algorithm used to implement Eqs. (15) and (16) is described in Sec. III C. In subsequent sections, for clarity, we call this correction the weighted average spin saturation (WASS) correction.

III. METHODS

III.A. fMRI time series simulation

Two simulated time series were derived from a synthetic high resolution $T2$-weighted volume with voxel dimensions $1 \times 1 \times 1$ mm^3, downloaded from the International Consortium of Brain Mapping[9] (ICBM). Each voxel in the volume

data was assumed to be an isochromat belonging to GM, WM, or CSF with known $T1$ values, 833, 500, and 2569 ms, respectively, as obtained from the ICBM website.[24] Head motion was simulated by rotating the $T2$-weighted volume in three-dimensional (3D) space prior to extracting each EPI slice, to form a fMRI volume. This process was repeated to obtain a set of time series volumes. The head was assumed to be moving in the scanner's frame of reference while the coordinates at which the EPI slice was imaged by the scanner were fixed. To mimic head motion such as nodding in a real subject, the motion included in-plane and out-of-plane rotations. Practically observed head rotations over successive volumes in the time series maintain continuity with previous head positions. Hence, the applied motion was designed to be smooth without being periodic.

To estimate the range of realistic through plane motion, real time MRI scans were obtained from a normal volunteer without head restraints using 2D turbo field echo in a Philips 3T system. The images were acquired while the subject was verbalizing words typically used in language tasks for fMRI studies. A hundred 140×108, 10 mm thick slices of the sagittal brain view were obtained with a dynamic scan time 251 ms. The relative range of interslice motion was estimated by registering each image to the initial image as a reference. Registration results indicated rotational and translational motion of up to $+/-5.4$ deg and $+/-5.2$ mm.

To consider the range of motion commonly used to evaluate most fMRI studies,[5,10] two time series were simulated with $+/-5$ and $+/-2$ deg rotational motion. The average magnitude of rotation between consecutive slice acquisitions was $0.25°$ and $0.09°$, respectively. Each time series consisted of 120 volumes with 14 slices in each volume. Three sets (one for each of the three coordinate axes x, y, z) of 121 iid random numbers were drawn from a uniform distribution to set the head position at the beginning of each volume acquisition. To ensure smoothness, a cubic polynomial was fit to the sequence of random angles for each coordinate axis. The orientation of the head during each intermediate EPI slice scan was obtained by sampling the polynomials at appropriate time points. The EPI time series parameters for both simulations were set at $TR=3000$ ms, $\alpha=90°$ using an interleaved slice acquisition. The given TR value and head trajectories constructed above determined the time instances at which every voxel in the $T2$ weighted MR volume was imaged by the scanner.

Spin saturation artifacts were introduced by treating each high resolution voxel as a WM, GM, or CSF isochromat. Consequently, Eqs. (4) and (7) were used to introduce spin saturation artifacts in the high resolution $T2$ volume. The activation task was assumed to be a block design, alternating a stimulus and a control cycle every 10 volumes. Activated voxels were created by increasing the intensities in manually marked regions of the volume by 2% before simulating motion and spin saturation artifacts. The synthetic activations were introduced such that activated EPI voxels would contain mainly GM and some WM isochromats. Voxels in an fMRI slice at a particular acquisition time instance were obtained by averaging the voxel intensities in the correspond-

ing $2 \times 2 \times 6$ neighborhood of the $T2$ volume. The resultant simulated time series consisted of 120 EPI volumes, with a voxel size of $2 \times 2 \times 6$ mm³. The ground truth activation map was obtained by down sampling the high resolution activation map to match the resolution of fMRI volumes. To account for signal noise Gaussian noise ($N(0,4)$) and Rayleigh noise ($\sigma=2$) were added to fMRI voxels with nonzero and no signal intensities, respectively.[11]

III.B. Map-slice-to-volume motion estimation and activation map computation

The MSV motion correction technique was introduced in our previous work and has shown improved localization of activation in human data.[6] Motion correction was performed by mapping each EPI slice on to a high resolution anatomical MR volume acquired in the same fMRI session, to accommodate interslice head motion. The MSV algorithm models 3D motion of multislice EPI data by allowing each slice to have its own six degrees of freedom, i.e., a rigid-body transform. Each EPI slice $h^{n_{\text{epi}}}$ is registered to a 3D anatomical reference volume g_{ref} using a rigid body transform denoted by $T_{\phi^{n_{\text{epi}}}}$. The vector $\phi^{n_{\text{epi}}}$ consists of six rigid motion parameters $t_x, t_y, t_z, \theta_x, \theta_y, \theta_z$ for EPI slice number n_{epi}. The automated registration finds this optimized transform $T_{\phi^{n_{\text{epi}}}}$ by maximizing the mutual information between $h^{n_{\text{epi}}}$ and g_{ref}. The MSV algorithm uses the Nelder–Mead downhill simplex optimizer.[12] The final set of optimized motion parameters and trilinear interpolation are used to transform and reconstruct each EPI slice $h^{n_{\text{epi}}}$ in the reference volume coordinate system.

Hypothesis testing of changes in voxel intensities of each time series after only MSV motion correction or both motion and WASS correction (described in the following section) was performed using 2000 random permutations.[2] The test statistic used was the student-T test of differences between stimulation and rest volumes. Activation maps were obtained by comparing the calculated p values with different alpha threshold values in the range of $[5 \times 10^{-4}, 1]$. Finally, ROC curves were generated by computing fractions of false positive and true positive counts relative to the known manually introduced activation pattern.

III.C. Weighted average spin saturation correction

The WASS correction proceeds in a sequential manner, processing each EPI slice indexed according to acquisition order by the same procedure. Similar to MSV, WASS correction uses a high resolution anatomical volume acquired during the same fMRI session. Each voxel in the anatomical volume is approximated by a GM, WM, or CSF isochromat with a corresponding approximate $T1$ and ρ_0 value. As described by the flow chart in Fig. 1, a "correction factor" value and a "time elapsed" counter is associated with each anatomical volume voxel. Each EPI slice is mapped onto the anatomical volume using the corresponding MSV motion estimates. This mapping is then used by the time elapsed counters to track the amount of time that has elapsed since the last time each anatomical voxel was excited. The correc-
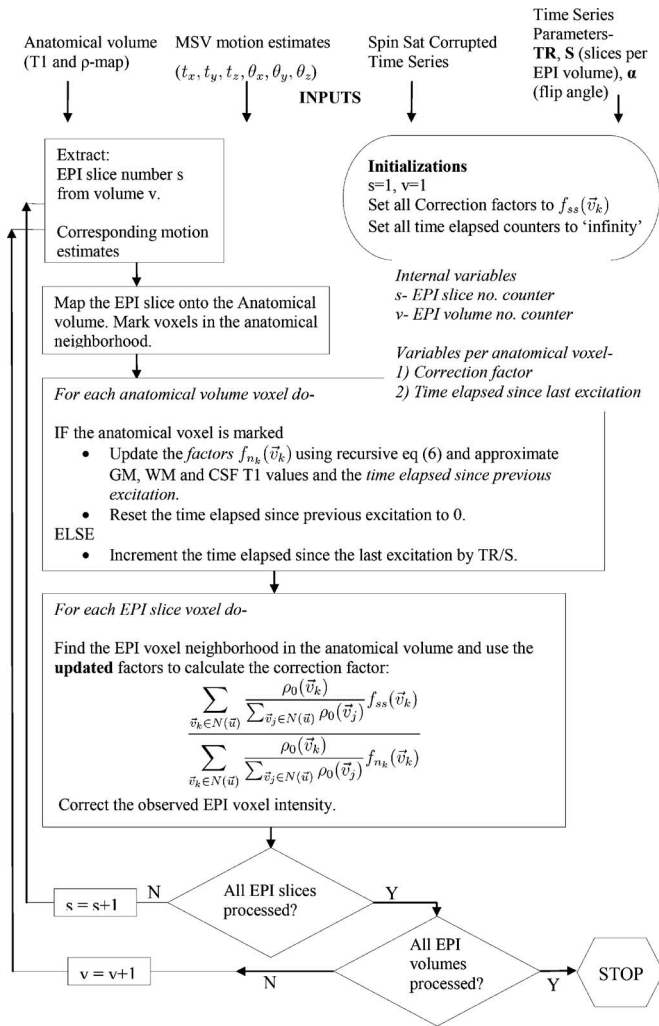
FIG. 1. Flowchart describing the implementation of WASS correction.

tion factor values $f_{n_k}(\vec{v}_k)$, $\vec{v}_k \in R$ for each anatomical volume voxel are recursively updated by Eq. (6), using the time elapsed counters and appropriate approximate $T1$ values. For a given EPI voxel in slice n_{epi} excited at time point $t_{n_{epi}}$, the factors $\hat{f}^{wa}_{n_{epi}}$ are computed using the updated correction factors f_{n_k} and approximate ρ_0 values in its anatomical neighborhood using Eq. (15). Each f_{n_k} in the anatomical neighborhood could have been updated a distinct number of times. This number of updates depends on the number of EPI slices that were mapped onto the anatomical voxel up to time $t_{n_{epi}}$. Since $\hat{f}^{wa}_{ss}$ is independent of the time between excitations, it can be computed straightforwardly using Eqs. (3) and (15). Lastly, the EPI voxel intensity is corrected using Eq. (16). This process is sequentially repeated for all the slices in the EPI time series.

For synthetic data we have access to an anatomical volume with the same accurate classification of GM, WM, and CSF, as that used to induce spin saturation artifacts. In reality spin saturation artifacts can be modeled as effects of the premature excitation of a collection of infinitesimally small isochromats in the vicinity of the EPI voxel. In the real data
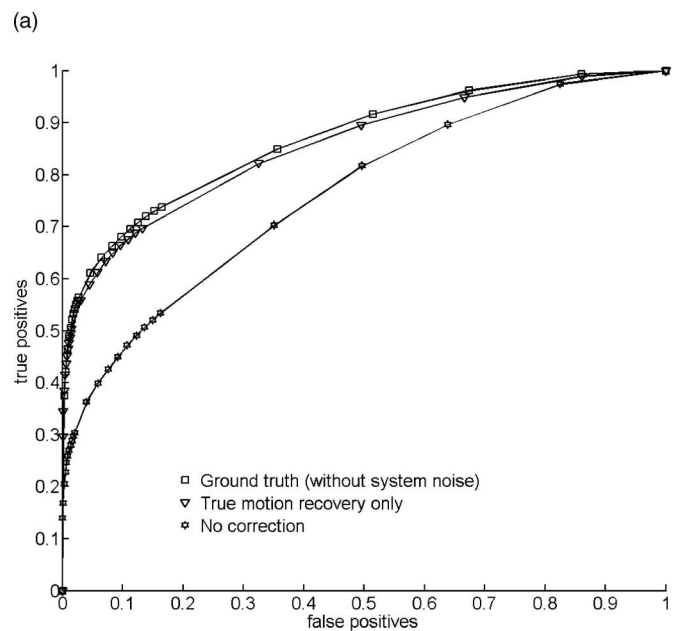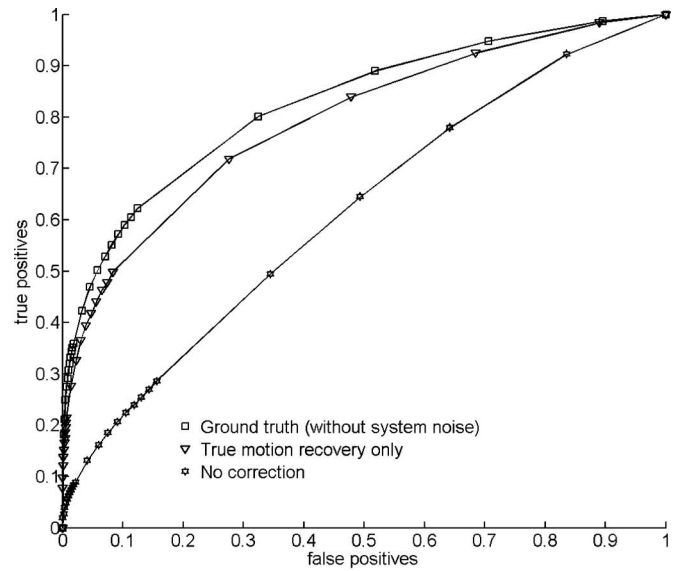

FIG. 2. ROC curve analyses of activated voxels from two time series simulated with head rotations of (a) $+/-5$ and (b) $+/-2$ deg (max/min). Plots are from the activation detection of simulated data with spin saturation and motion artifacts after no correction and after true motion recovery only ($\triangledown$). "Ground truth" ($\square$) is from a time series simulated with only motion without spin saturation artifacts after true motion recovery.

case, due to the finite resolution of the anatomical volume, there is an inherent inaccuracy in the classification of GM, WM, and CSF isochromats. To account for the effect of this error in classification in our WASS correction, a "blurred" ICBM $T1$ volume was used as the anatomical volume. This volume was created by roughly approximating the dominant $T1$ classification over three voxels (i.e., 3 mm) along the z axis, using a $1 \times 1 \times 3$ mm^3 resolution $T1$ volume from the ICBM website.[24] The misclassification was applied only along the longitudinal direction as spin saturation artifacts occur mainly due to out-of-plane motion.[1] In contrast, the

TABLE I. Approximate area under the ROC curve (AUC) values comparing the improvement in activation detection for the manually introduced activation pattern after true motion correction only. The difference in AUC between ground truth and only motion correction can be attributed to the loss due to spin saturation artifacts. The loss is denoted as a % value relative to the AUC difference between "only motion correction" and "no correction."

	No correction	Ground truth	Only motion correction	Reduction in the AUC due to spin saturation
+/−5°	0.614	0.826	0.793	0.033(18.4%)
+/−2°	0.763	0.868	0.856	0.012(12.9%)

time series simulation process used a high resolution $T1$ volume ($1 \times 1 \times 1$ mm^3) for the tissue classification.

IV. RESULTS

Two fMRI time series simulated using (max/min) +/−5 and +/−2 deg rotational motion trajectories with corresponding spin saturation artifacts were treated as "observed" time series data. Similarly two corresponding time series free of the spin saturation effect were also generated using the same motion trajectories. These time series were corrected using known true motion, to establish ground truth data.

The effect of only spin saturation artifacts on activation detection was evaluated by correcting both observed time series for motion only using the known true motion parameters. Corresponding ROC curves are shown in Figs. 2(a) and 2(b). The degrading effect of spin saturation artifacts on activation detection was quantified by computing the area under the curve (AUC) values for both ROC curves, listed in Table I. As motion was reduced from +/−5 to +/−2 deg, the effect of spin saturation reduced almost proportionately. This can be seen by the loss of 0.033 and 0.012 in corresponding AUC values due to spin saturation alone. Activation maps showing the effect of spin saturation artifacts on activation detection for the simulated time series with (a) +/−5 and (b) +/−2 deg rotation motion are shown in Figs. 3(a) and 3(b), respectively.

In reality, the $T1$ values for GM, WM, and CSF vary across the subject population and are known only approximately. Three WASS corrections were performed with (1) exact ICBM $T1$ values, $T1_{GM}=833$ ms, $T1_{WM}=500$ ms, and $T1_{CSF}=2569$ ms, (2) approximate (text book) $T1$ values,[8] $T1_{GM}=900$ ms, $T1_{WM}=600$ ms, and $T1_{CSF}=4000$ ms, and (3) a single $T1$ value, $T1_{GM}=833$ ms. Average percentage errors in the corrected voxel intensities were obtained, using the ground truth intensities, as follows:

$$\text{Avg. \% error} = \frac{1}{N}\sum_{i=1}^{N} \frac{|I_{\text{true}}(\vec{u}_i) - \hat{I}_{\text{true}}(\vec{u}_i)|}{I_{\text{true}}(\vec{u}_i)}, \qquad (17)$$

where N is the number of non-zero intensity voxels in the region of interest (ROI) for each fMRI volume. $\hat{I}_{\text{true}}(\vec{u})$ is the spin saturation compensated intensity at coordinate $\vec{u}$ in the WASS corrected time series and $I_{\text{true}}(\vec{u})$ is the corresponding known true intensity obtained from the ground truth time series. The ROI was restricted to the manually introduced
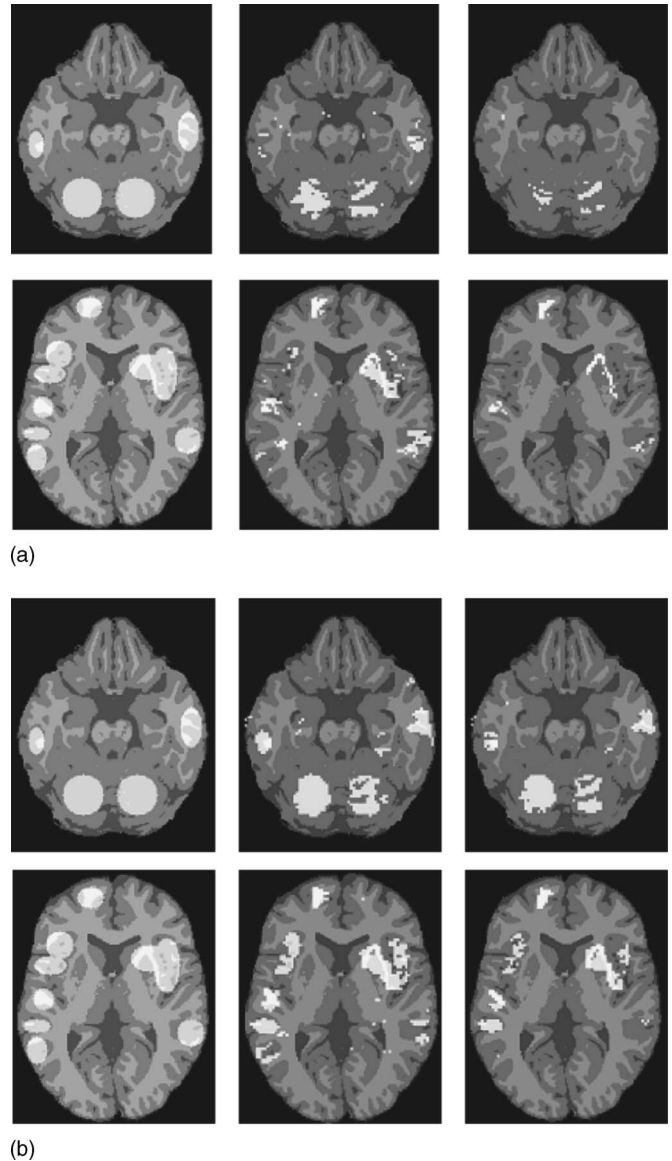
(a)

(b)

FIG. 3. Activation maps (alpha=0.002) from the simulated time series with (a) +/−5 and (b) +/−2 deg rotation motion superimposed on the anatomical $T1$-weighted volume. Images in rows show two selected slices showing: the manually applied true activation pattern (first column), activation maps computed for simulated time series without spin saturation after only true motion correction (second column), and for corresponding simulated time series with spin saturation after only true motion correction (third column).

activation regions. Error standard deviation and max/min percentage intensity error values listed in Table II indicate a reduction in intensity errors following WASS correction. Reduction is errors after WASS correction using approximate $T1$ values was comparable to that using exact $T1$ values. Further, for the larger $[-5,5]$ range of motion WASS correction using approximate $T1$ values significantly out performed that using a single $T1$ value, in contrast this improvement in performance was noticeably smaller for the $[-2,2]$ motion range.

The viability of WASS depends on its ability to withstand the combined effect of errors in interslice motion estimation, approximate $T1$ values, and approximate relative proton den-

TABLE II. Improvement in percentage intensity errors following WASS correction (using exact $T1$ values, approximate $T1$ values, and a single (exact GM) $T1$ value) for simulated data with ± 5 and ± 2 deg rotational motion and spin saturation artifacts. Comparisons were restricted to the manually added activation regions. The table lists max/min and standard deviation (SD) values of percentage intensity errors computed using Eq. (17) with respect to corresponding ground truth data.

| | | WA-spin saturation correction using | | |
	No spin saturation correction	Exact $T1$s	Approximate $T1$s	Single (exact) $T1$s
$\pm -5°$				
max/min	5.3663/0.2891	1.0189/0.0638	1.3862/0.0834	2.5124/0.1278
SD	1.2032	0.1905	0.2858	0.5221
$\pm -2°$				
max/min	2.3093/0.0936	0.5472/0.0263	0.7210/0.0332	1.1220/0.0526
SD	0.4996	0.1130	0.1467	0.2206

sities. Motion estimates for both observed time series with signal noise and $[-5,5]$ and $[-2,2]$ deg rotational motion ranges were obtained using the MSV algorithm. Root-mean-square errors (RMSE) between MSV motion estimates and the known true motion in Table III show subvoxel accuracy in both cases. Intensity modulation due to the spin saturation effect did not significantly affect the accuracy of MSV. These motion estimates were then used to process both time series using WASS correction. WASS correction was performed using exact (ICBM $T1s$), approximate (textbook $T1s$), and a single (ICBM GM) $T1$. To study the efficacy of WASS using MSV motion estimates, ROC curves were generated for both observed time series after MSV motion correction with and without WASS correction. ROC plots in Fig. 4 and corresponding AUC values in Table IV show that WASS correction based on MSV motion estimates significantly improved activation detection compared to motion only correction.

Activation maps (alpha=0.001) for two representative slices from both observed time series before and after WASS correction in Figs. 5(a) and 5(b) show that WASS correction clearly improves activation detection. For the data with +/−5 deg motion [Fig. 5(a)], activation maps indicate that WASS using approximate $T1_{GM}$, $T1_{WM}$, and $T1_{CSF}$ values performs better than that using a single $T1$ (exact $T1_{GM}$) correction for some activation patterns. In contrast, there appears to be little perceptible difference in the efficacy of the correction with approximate and single $T1s$ for the data with smaller motion [Fig. 5(b)]. This is consistent with our earlier observation concerning residual percentage intensity errors after WASS correction using different approximate $T1$ values shown in Table II.

V. DISCUSSION

We have developed a spin saturation artifact correction method for fMRI time-series data. Its performance was evaluated using ROC curves, activation maps, and simulated fMRI time-series data. In contrast to commonly used volume-to-volume fMRI registration, we employ a MI based MSV registration algorithm. MSV estimates rigid motion parameters by mapping each EPI slice in the time series onto a high resolution anatomical volume obtained from the same subject. This mapping is used to obtain information about the tissue composition of each low resolution EPI voxel using the high resolution anatomical volume. After identification of spin saturation affected EPI voxels, WASS correction uses the knowledge of percentage contributions of different brain tissues (i.e., WM, GM, and CSF) to the EPI voxel intensity, to compensate it for spin saturation effects.

Inherent GM, WM, and CSF misclassifications, approximate $T1$ values and approximate proton density values were used in the WASS correction based on MSV motion estimates. Apart from its dependence on the accuracy of MSV motion estimates, the efficacy of the WASS correction for EPI voxels in slice n_{epi}, is largely a function of the estimates of the correction factors $\hat{f}_{ss}^{wa}(.)$ and $\hat{f}_{n_{epi}}^{wa}(.)$ in Eq. (15). These estimates improve with the resolution of the anatomical volume with respect to EPI volumes.

The range of motion in a fMRI time series varies with the level of corporation from a subject as well as the tasks being studied. Typically volumetric registration motion estimates of up to +/−1 mm translation and +/−1 deg rotation have been reported for normal subjects.[1] In contrast, MSV regis-

TABLE III. RMSE values between the applied ground truth motion and the motion estimates recovered by MI based MSV for both simulated time series. The values are representative of the subpixel accuracy of the MSV registration method.

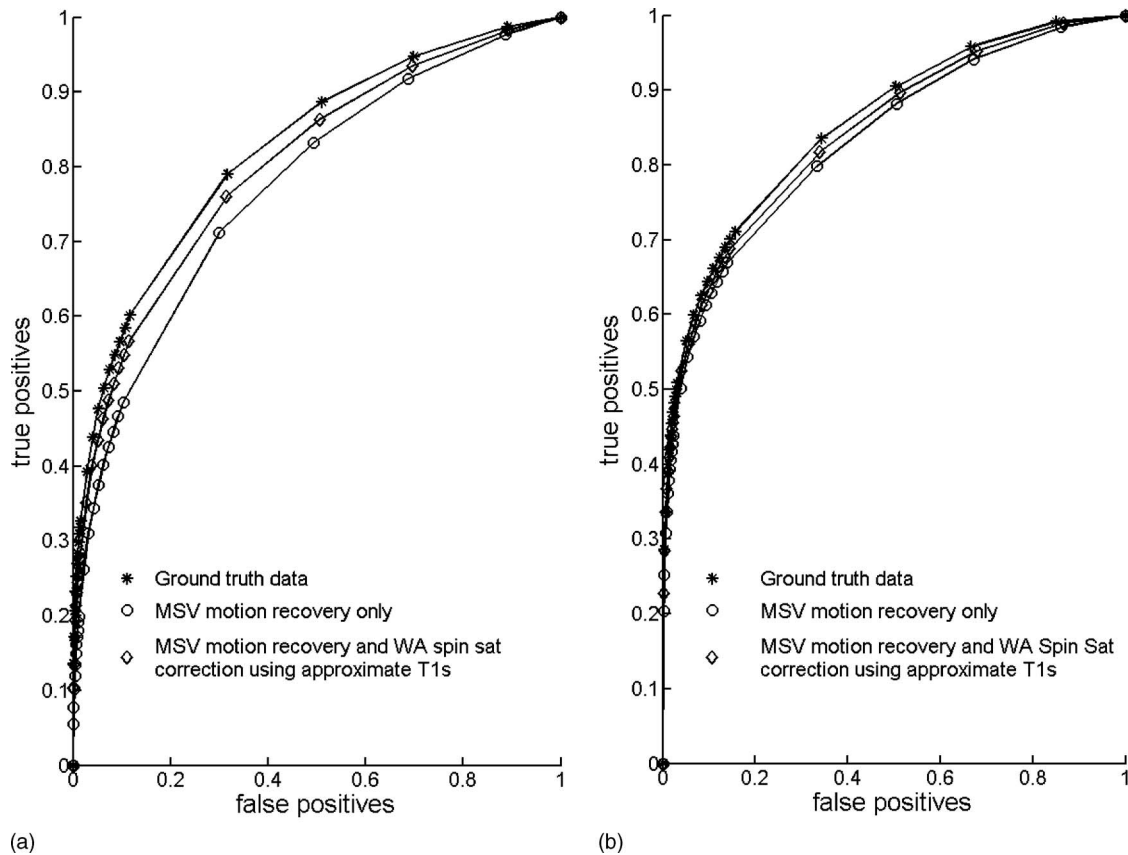| | Rotation RMSE (deg) | | | Translation RMSE (mm) | | |
	R_x	R_y	R_z	T_x	T_y	T_z
+/−5°	0.3555	0.3402	0.0908	0.1627	0.1796	0.1787
+/−2°	0.2187	0.2067	0.1278	0.1257	0.1449	0.1345

FIG. 4. ROC curve analyses of activation detection from two noisy time series simulated with head rotations of (a) $+/-5$ and (b) $+/-2$ deg (max/min), for data processed with MSV only (○) and both MSV and WASS (◇). Ground truth (*) is from a time series simulated with only motion parameters without spin saturation effect, after true motion recovery. The WASS correction used MSV motion estimates and approximate tissue $T1$ values.

tration results have estimated head motion of up to 4.1 mm translations and 7.3 deg rotations.[6] Motion for certain fMRI studies, such as verbal tasks, may be larger than the typically observed subject motion due to jaw and mouth movements. For a realistic motion range, $[-5,5]$, our results in Table IV show that the proposed spin saturation artifact correction provides significant improvement in activation detection. This is quantified by an increase in the AUC of the ROC curve from 0.77 before WASS correction to 0.8 after WASS correction. This improvement is consistent with the effect of spin saturation artifacts on activation analysis shown in Table I. For the time series with a smaller range of motion, $[-2,2]$, the effect is relatively smaller, but still proves to be

effective when the activation maps are compared. Our previous study[6] and the motion assessment in this study using real time dynamic MRI data indicate that the range of $+/-5$ is a realistic representation of subject head motion.

$T1$ values for GM, WM, and CSF vary across the patient population. Table II summarizes results of the study of the effect of error in $T1$ values on WASS correction. These results indicate that WASS correction using approximate $T1$ values shows reduced accuracy when compared to that using exact $T1s$. However, WASS correction using approximate $T1$ values significantly reduces residual errors in corrected voxel intensities when compared to that using a single $T1$. The WASS correction using approximate $T1$ values reduces re-

TABLE IV. Approximate area under the ROC curve (AUC) values demonstrating improved activation detection for the noisy simulated fMRI time series, following both MSV motion and WASS correction. The "approximate $T1s$" column tries to emulate postprocessing in a realistic scenario, where only MSV motion estimates and approximate $T1$ values are available. The percentage values in the approximate $T1s$ column denote the improvement in AUC values due to WASS correction alone, as a percentage of that obtained by Only MSV Motion Correction. The improvements in AUC were calculated with respect to the no correction AUC in Table I.

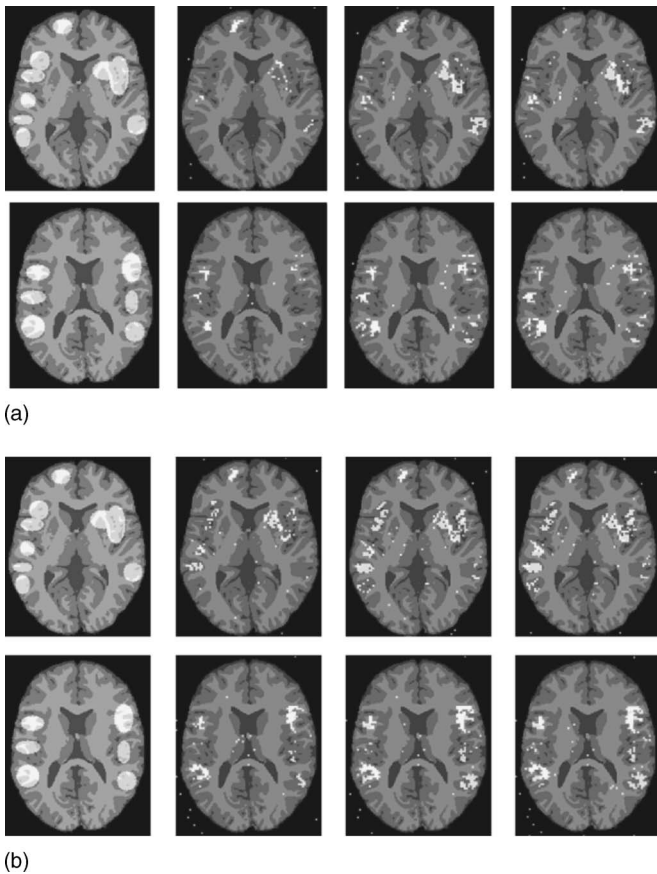| | Ground truth (noisy) | Only MSV motion correction | MSV motion and WASS correction | | |
			Exact $T1s$	Approximate $T1s$	Single $T1s$
$+/-5°$	0.822	0.774	0.800	0.802(17.4%)	0.803
$+/-2°$	0.855	0.834	0.845	0.845(12.2%)	0.844

(a)

(b)

FIG. 5. Sample activation maps (alpha=0.001) comparing the effect of WASS correction using approximate $T1$ values on activation detection for two simulated time series with (a) +/−5 and (b) +/−2 deg motion and signal noise. Both time series were corrected using MSV motion estimates and corresponding WASS correction. For comparison, two sample slices are shown from: the manually applied true activation pattern (first column), corresponding activation maps after only MSV based motion correction, i.e., no WASS correction (second column), after MSV motion followed by WASS correction with approximate $T1$ values (third column), and after MSV motion followed by WASS correction with a single $T1$ value (fourth column).

sidual percentage intensity errors from 5% to 1.5%. As the $T1_{CSF}$ time constant is significantly different from $T1_{GM}$ and $T1_{WM}$, misclassifications of CSF as GM or WM will contribute strongly to the error metric in Eq. (17). Since WASS using a single $T1$ uses only the $T1$ value of GM in our comparison, inclusion of CSF in the ROI may bias this error metric toward WASS using distinct $T1_{GM}$, $T1_{WM}$, and $T1_{CSF}$ values. Hence, to account for the prevalence of activation in GM, we restrict the ROI in Eq. (17) to the manually introduced activation pattern only.

While the effect of inaccuracies in $T1$ values, proton density values, motion estimates, and classification of GM, WM, and CSF isochromats was accounted for in the evaluation of our WASS correction, the slice profile in both the simulation and the correction was assumed to be rectangular. WASS correction depends on the cosine of effective flip angles at the resolution of the anatomical volume, as modeled by Eqs. (3) and (6). Thus, errors in approximations to the actual slice profile used to acquire the EPI time series may affect the performance of our spin saturation correction.

This study focuses on demonstrating the viability of a new spin saturation correction technique based on MSV motion estimates and evaluating its performance using realistically simulated mathematical phantom data and corresponding ground truth. While validation using real time series would be ideal, establishing ground truth for a real fMRI time series can be a challenging task. Approximations and inaccuracies that are representative of clinical human data were introduced in the evaluation of our WASS correction method.

To be consistent with the multi-slice acquisition protocol, each fMRI slice was subjected to a different but continuous set of head motion parameters and associated spin saturation artifacts. While head motion may induce changes in field inhomogeneity and result in related geometric distortions of EPI data, our WASS correction method is to be applied after correction for such field inhomogeneity artifacts.[13–16] Furthermore, slice-to-volume registration can be adapted to estimate nonlinear warps for geometric distortion correction.[17,18] Lastly, the WASS correction scheme can be modified to be applied using nonlinear warps; with reference to Fig. 1, the input rigid motion parameters can be replaced by warp estimates, leaving much of the algorithm unaltered.

Motion correction approaches using volume to volume registration are not designed to detect subject head motion between slice acquisitions correctly. Numerous fMRI analysis techniques, apply the same rigid transform to the whole volume[19–21] allowing no interslice motion. Further many use $L2$ metrics which have been shown to result in spurious motion estimates in the presence of activation.[10,22] Since spin saturation artifacts have magnitudes comparable to activation,[23] these methods may give erroneous motion estimates for time series data leading to false detection of activation. For a given EPI scan with known TR, TE, and flip angle values, MSV motion estimates can conceivably be used to correct for motion and spin saturation effects in fMRI time series using WASS correction. However, the success of the correction rests on the ability of MSV to estimate motion accurately in fMRI data corrupted by spin saturation artifacts.

ACKNOWLEDGMENTS

a)Electronic mail: rbhagali@umich.edu

[1] K. J. Friston, S. Williams, R. Howard, R. S. Frackowiak, and R. Turner, "Movement-related effects in fMRI time-series," Magn. Reson. Med. **35**, 346–355 (1996).
[2] T. E. Nichols and A. P. Holmes, "Nonparametric permutation tests for functional neuroimaging: A primer with examples," Hum. Brain Mapp. **15**, 1–25 (2002).
[3] K. J. Friston, A. P. Holmes, J. B. Poline, P. J. Grasby, S. C. Williams, R. S. Frackowiak, and R. Turner, "Analysis of fMRI time-series revisited,"

Neuroimage **2**, 45–53 (1995).

[4] K. Friston, P. Jezzard, and R. Turner, "Analysis of functional MRI time-series," Hum. Brain Mapp. **1**, 153–171 (1994).

[5] L. Muresan, R. Renken, J. Roerdink, and H. Duifhuis, "Automated correction of spin-history related motion artefacts in fMRI: Simulated and phantom data," IEEE Trans. Biomed. Eng. **52**, 1450–1460 (2005).

[6] B. Kim, J. Boes, P. Bland and T. Chenevert, and C. Meyer, "Motion correction in fMRI via registration of individual slices into an anatomical volume," Magn. Reson. Med. **41**, 964–972 (1999).

[7] W. Hinshaw and A. Lent, "An introduction to NMR imaging: From the Bloch equation to the imaging equation," Proc. IEEE **71**, 3 (1983).

[8] E. Haacke, R. Brown, M. Thompson, and R. Venkatesan, *Magnetic Resonance Imaging: Physical Principles and Sequence Design* (Wiley, New York, 1999).

[9] C. Cocosco, V. Kollokian, R. Kwan, and A. Evans, "Brain web: Online interface to a 3D MRI simulated brain database," Neuroimage **5**, S425 (1997).

[10] L. Freire, A. Roche, and J.-F. Mangin, "What is the best similarity measure for motion correction in fMRI time series?," IEEE Trans. Med. Imaging **21**, 470–484 (2002).

[11] D. G. Nishimura, *Principles of Magnetic Resonance Imaging* (Stanford University Press, Stanford, 1996).

[12] J. A. Nelder and R. Mead, "A simplex method for function minimization," Comput. J. **7**, 308–313 (1965).

[13] P. Munger, G. Crelier, T. Peters, and G. Pike, "An inverse problem approach to the correction of distortion in EPI images," IEEE Trans. Med. Imaging **19**, 681–689 (2000).

[14] R. Cusack, M. Brett, and K. Osswald, "An evaluation of the use of magnetic field-maps to undistort echo-planar images," Neuroimage **18**, 127–142 (2003).

[15] V. Roopchansingh, R. Cox, A. Jesmanowicz, B. Ward, and J. Hyde, "Single-shot magnetic field mapping embedded in echo-planar time-course imaging," Magn. Reson. Med. **50**, 839–843 (2003).

[16] D. Yoder, Y. Zhao, C. Paschal, and J. Fitzpatrick, "MRI simulator with object-specific field map calculations," Magn. Reson. Imaging **22**, 315–328 (2004).

[17] J. Kybic, P. Thevenaz, A. Nirkko, and M. Unser, "Unwarping of unidirectionally distorted EPI images," IEEE Trans. Med. Imaging **19**, 80–93 (2000).

[18] B. Kim, J. L. Boes, K. A. Frey, and C. R. Meyer, "Mutual information for automated multimodal image warping: Visualization in Biomedical Computing," Lect. Notes Comput. Sci. **1131**, 349–354 (1996).

[19] R. P. Woods, S. R. Cherry, and J. C. Mazziotta, "Rapid automated algorithm for aligning and reslicing PET images," J. Comput. Assist. Tomogr. **16**, 620–633 (1992).

[20] Functional Imaging Laboratory, Statistical Parametric Mapping: SPM 2. Wellcome Department of Imaging Neuroscience, May 2003, available at http://www.fil.ion.ucl.ac.uk/spm/spm2.html.

[21] K. J. Friston, J. Ashburner, C. D. Frith, J.-B. Poline, J. D. Heather, and R. S. J. Frackowiak, "Spatial registration and normalization of images," Hum. Brain Mapp. **3**, 165–189 (1995).

[22] L. Freire and J.-F. Mangin, "Two-stage alignment of fMRI time series using the experiment profile to discard activation-related bias, MICCAI 2002," Lect. Notes Comput. Sci. **2489**, 663–670 (2002).

[23] L. Muresan, R. Renken, J. Roerdink, and H. Duifhuis, "Position-history and spin-history artifacts in fMRI time-series. Medical imaging 2002: Physiology and function from multidimensional images," Proc. SPIE **4683**, 444–451 (2002).

[24] ICBM website, www.bic.mni.mcgill.ca/brainweb/.